RAIRO-Oper. Res. 56 (2022) 3689–3709
https://doi.org/10.1051/ro/2022168

RAIRO Operations Research
www.rairo-ro.org

COUPLED COMPLEX BOUNDARY METHOD FOR A GEOMETRIC INVERSE SOURCE PROBLEM

Lekbir Afraites*, Chorouk Masnaoui and Mourad Nachaoui

Abstract. This work deals with a geometric inverse source problem. It consists in recovering the characteristic function of an unknown inclusion based on boundary measurements. We propose a new reconstruction method based on the CCBM and the shape gradient method, the inverse problem is formulated as a shape optimization one, corresponding to a coupled complex boundary state problem. Well posedness and existence results are presented. A computed expression for the shape gradient is used to implement a gradient algorithm. The efficiency and accuracy of the reconstruction algorithm are illustrated by some numerical results, and a comparison between CCBM, Least-squares and Kohn-Vogeluis methods is presented.

Mathematics Subject Classification. 65K05, 65K10, 49J20, 49J50.

Received December 27, 2021. Accepted September 24, 2022.

1. Introduction

Inverse source problems is a class of inverse problems that aims to find (u, F) solution of the equation $Lu = F$ in Ω, using a pair of additional data on the boundary $\partial\Omega$ of an open bounded set Ω, where L is an elliptic linear differential operator and F is the unknown source term. It is well known that this problem is one of the highly ill-posed problems in Hadamard sense [10], therefore, a general source function cannot be identified uniquely using boundary measurements, see [22] and [13].

A particular source problem where the unknown source F is of the form $p\chi_\omega$ (χ is the characteristic function) has been studied by Afraites *et al.* [5] using a shape optimization reformulation, the unknown source support was reconstructed by a gradient algorithm using the shape gradient and the adjoint method, then the stability study was presented. This problem has been studied also by Hrizi and Hassine [20] using a topological optimization formulation, the unknown source was reconstructed using a level-set curve of the topological gradient. Kress and Rundell [21] presented an iterative solution method *via* boundary integral equations, by reformulating the inverse source problem as an inverse boundary value problem with a non-local Robin condition on the boundary of the source domain. In [27] a method for the reconstruction of star-shaped characteristic sources was developped, by reducing the problem to an algebraic system of equations. The paper [6] traited the inverse characteristic source problem, in the case of Helmholtz equations, from the determination of the

Keywords. Coupled complex boundary method, inverse geometric source problem, shape optimization, shape derivative, adjoint method.

Faculty of Sciences and Techniques, Sultan Moulay Slimane University, Beni Mellal, Morocco.
*Corresponding author: lekbir.afraites@gmail.com

barycenter of the characteristic source and the recovery of its geometry from a class of star-shaped characteristic sources, using an algorithm based on an equivalent reciprocity functional formulation. El Badia and Nara [14] have also investigated the inverse source problem of the Helmholtz equation, where the source consists of multiple point sources, an algebraic algorithm was proposed to identify the number, locations and intensities of the point sources from boundary measurements. This inverse source problem was studied also by a coupled complex boundary method (CCBM), originally proposed by Cheng *et al.* in [9], it consists in recovering the source term p in the equation $Lu = p\chi_\omega$, when the source support ω is known, using some additional Dirichlet and Neumann boundary conditions. The method consists in coupling the two conditions in a single complex Robin boundary condition, and then the boundary data fitting is recast into the whole domain data fitting. The authors have shown that the new CCBM method makes the inverse source problem more robust and more efficient in computations. Our aim here is to apply this CCBM method to a geometric Inverse source problem, we should reconstruct the source support ω rather than the function p, and we consider the more general case $Lu = h_1\chi_\omega + h_2\chi_{\Omega\setminus\overline{\omega}}$, for some given source functions h_1 and h_2.

Recently, the idea of using the coupled complex boundary method for solving inverse geometric problem was proposed in [1] for solving inverse obstacle problem, the author have shown that the proposed method is feasible and effective for such problems.

To fix ideas, let Ω be an open, bounded, and connected subset of $\mathbb{R}^d$ ($d = 2$ or 3) with $\mathcal{C}^1$ boundary $\partial\Omega$. Let δ be a positive constant, we define the set of admissible domains denoted by Ω_δ as the set of all open simply connected subdomains ω of Ω with a $\mathcal{C}^{2,1}$ boundary, such that $d(x, \partial\Omega) > \delta$ for all $x \in \omega$. The notation χ_ω denotes the characteristic function of ω. For some given functions $h_1, h_2 \in L^2(\Omega)$, and based on some knowledge on the boundary conditions, namely the voltage $f \in H^{\frac{1}{2}}(\partial\Omega)$ and the current measurement $g \in H^{-\frac{1}{2}}(\partial\Omega)$, we try to find ω and u solution of the following overdetermined problem

$$\begin{cases} -\Delta u + \alpha u = h_1\chi_\omega + h_2\chi_{\Omega\setminus\overline{\omega}} & \text{in} \quad \Omega, \\ u = f & \text{on} \quad \partial\Omega, \\ \partial_n u = g & \text{on} \quad \partial\Omega, \end{cases} \tag{1}$$

where ∂_n stands for the outward normal derivative, and α is a non-negative constant.
To be more precise, the inverse source problem is reformulated as follows:

Problem 1.1.

$$\textit{find} \quad \omega \in \Omega_\delta \quad \textit{and} \quad u \quad \textit{which satisfy the overdetmined system} \quad (1). \tag{2}$$

Note that the right-hand side of the first equation in (1) can be re-expressed as $h_2 + (h_1 - h_2)\chi_\omega$.
Among the existing methods found in the literature, a robust reconstruction of the unknown inclusion consists in reformulating the inverse problem (1) into the following least-squares minimization problem (see for example [4, 15])

$$J_{LS}(\omega) = \frac{1}{2}\int_{\partial\Omega} |u_n - f|^2, \tag{3}$$

where f is the boundary measurement and u_n is the state function that solves

$$\begin{cases} -\Delta u_n + \alpha u_n = h_1\chi_\omega + h_2\chi_{\Omega\setminus\overline{\omega}} & \text{in} \quad \Omega, \\ \partial_n u_n = g & \text{on} \quad \partial\Omega, \end{cases} \tag{4}$$

Another well known optimization approach is based on minimizing a Kohn-Vogelius functional (see [3, 4, 8]), which illustrates a more robust optimization performances, through the following optimization problem

$$J_{KV}(\omega) = \frac{1}{2}\int_\Omega |\nabla(u_d - u_n)|^2 + \frac{\alpha}{2}\int_\Omega |u_d - u_n|^2, \tag{5}$$

and by splitting the over-determined boundary value problem (1) in two auxiliary problems. We denote by u_n the solution of the first one (4) associated to the Neumann data g, and u_d is the solution of the second one

associated to the Dirichlet data f given by

$$\begin{cases} -\Delta u_d + \alpha u_d = h_1\chi_\omega + h_2\chi_{\Omega\setminus\overline{\omega}} & \text{in } \Omega, \\ u_d = f & \text{on } \partial\Omega. \end{cases} \tag{6}$$

We note from the above statements that the minimization problems (3) and (5) use the Neumann data g and the Dirichlet data f sequentially. In this paper, we propose a new coupled complex boundary method (CCBM) that uses both g and f data in a single PDE. The idea of the CCBM is to couple the Neumann data and Dirichlet data in a Robin boundary condition in such a way that the Neumann data and Dirichlet data are the real part and imaginary part of the Robin boundary condition, respectively. As a result, the data needed to fit defined on the boundary $\partial\Omega$ are transferred to the volume problem defined on Ω. The coupled complex boundary method (CCBM) was first proposed by Cheng *et al.* in ([9]) for solving an inverse source problem, Rongfang *et al.* in ([17] applied it to an inverse conductivity problem with one measurement. More recently, this method was also applied in solving inverse obstacle problems by Afraites in [1] and used for solving stationary free boundary problems by Rabago [26]. To the best of our knowledge, in the literature, this is the first time that the idea of the coupled complex boundary condition has been explored for solving geometric inverse source problem.
Unlike the classical methods, the CCBM method allows us to define the cost function J in the whole domain Ω which brings advantages of robustness in the reconstruction compared to the Least-Squares type functions which are defined only on the boundary. From a theoretical perspective, it is difficult to prove the superiority of the proposed Complex coupled formulation over the Kohn-Vogeluis one. However, numerical examples in Section 6 indicate that it leads to more robust reconstruction results for this geometric inverse source problem.

The outline of this paper is organized as follows. In Section 2, we present the new coupled complex boundary method appropriate to our geometric inverse source problem and its reformulation at the shape optimization by introducing the regularized Least Squares fitting for the imaginary part of the complex PDE's solution . In Section 3, we present the well-posedness result of the direct problem. Section 4 is devoted to the existence of an optimal solution of our minimization problem. In Section 5 we establish the shape gradient calculus of the cost function. In the Section 6, we give an algorithm based on the gradient method and we solve an elliptic problem in order to find the steepest descend direction in the space of H^1 velocity vector field that satisfies certain boundary conditions. Then, we present detailed numerical results. Finally, we present the conclusion in Section 7 and elaborate the calculation of the shape state derivative in the appendix in Section 8.

2. Coupled complex boundary problem

From now onwards, we will use the following notations, we denote by $H^m(G)$ the Sobolev space of order m, which consist of the complex-valued functions defined on a domain $G \subset \mathbb{R}^d$, given by

$$H^m(G) := \{v \in L^2(G) :\ D^k v \in L^2(G),\ \forall k \in \mathbb{N}^d,\ |k| \le m\}.$$

Thus $H^0(G) := L^2(G)$. The Hilbert space $H^m(G)$ is equipped with the scalar product

$$\langle u, v\rangle_{m,G} := \sum_{|k|\le m} \int_G D^k u\, \overline{D^k v}\, dx \quad \forall u, v \in H^m(G),$$

and the norm $\|u\|_{m,G} := \langle u, u\rangle_{m,G}^{1/2} \quad \forall u \in H^m(G)$. We denote by i the imaginary unit.
Combining the Dirichlet and Neumann boundary data in a complex Robin boundary condition, the problem (1) is transferred into the following complex boundary value problem

$$\begin{cases} -\Delta u + \alpha u = h_1\chi_\omega + h_2\chi_{\Omega\setminus\overline{\omega}} & \text{in } \Omega, \\ \partial_n u + iu = g + if & \text{on } \partial\Omega. \end{cases} \tag{7}$$

Then, for a solution of (7), $u = u_1 + iu_2$, the real and imaginary parts of u satisfy

$$\begin{cases} -\Delta u_1 + \alpha u_1 = h_1\chi_\omega + h_2\chi_{\Omega\setminus\overline{\omega}} & \text{in} \quad \Omega, \\ \partial_n u_1 - u_2 = g & \text{on} \quad \partial\Omega. \end{cases} \tag{8}$$

$$\begin{cases} -\Delta u_2 + \alpha u_2 = 0 & \text{in} \quad \Omega, \\ \partial_n u_2 + u_1 = f & \text{on} \quad \partial\Omega. \end{cases} \tag{9}$$

Remark 2.1. Obviously, if (ω, u) satisfies (1), then (7) holds. Conversely, if $u_2 = 0$ in Ω, then $u_2 = \partial_n u_2 = 0$ on $\partial\Omega$, from (8) and (9), it follows that $(\omega, u) = (\omega, u_1)$ satisfies (1).

From the above discussion, the Problem 1.1 is equivalent to the following inverse problem:

Problem 2.2. *Given* $(f, g) \in L^2(\partial\Omega) \times L^2(\partial\Omega)$ *and* $(h_1, h_2) \in L^2(\Omega) \times L^2(\Omega)$, *find* $(\omega, u) \in \Omega_\delta \times H^1(\Omega)$ *such that*

$$u_2 = 0 \quad \text{in } \Omega,$$

where u_2 *is the imaginary part of the solution* $u = u_1 + iu_2$ *of the complex boundary problem (7).*

To solve the inverse shape Problem 2.2, we transform it into the following shape optimization functional:

$$J(\omega) = \frac{1}{2}\|u_2\|^2_{0,\Omega}, \tag{10}$$

and introduce the following minimization problem, find $\omega^* \in \Omega_\delta$ an admissible shape, such that

$$\omega^* = \inf_{\omega \subset \Omega_\delta} J(\omega). \tag{11}$$

This problems is unstable under data perturbations. Indeed, the choice of low frequency in measurements data can often be interpreted as a regularization method. But additional regularization is usually recommended to stabilize the numerical algorithm and obtain a satisfactory reconstruction. Thus, we consider the following regularized shape functional

$$J(\omega) = \frac{1}{2}\|u_2\|^2_{0,\Omega} + \varepsilon P_\Omega(\omega), \tag{12}$$

where $P_\Omega(\omega)$ is the perimeter of ω relative to Ω ([25], page 48), and ε is a regularization parameter (see [2, 24] for the choice of the latter).

Remark 2.3. The new method allows us to define the cost function J in the whole domain Ω which brings advantages of robustness in the reconstruction such as the Kohn-Vogelius cost function J_{KV} compared to the Least Squares fitting J_{LS} which is defined only on the boundary $\partial\Omega$ (see [4,5]). Compared to the Kohn-Vogelius method, the latter requires two problems to be solved at each iteration, however the new method (CCBM), needs a single complex problem to be solved.

3. Well-posedness result

Before discussing the existence of solution to our problem, we first study the well-posedness of the forward complex problem (*i.e.*, existence, uniqueness, and sensitivity to data).

Using Green's formula we derive the variational formulation for (7)

$$\text{Find} \quad u \in H^1(\Omega), \quad \text{such that} \quad a(u, v) = l(v), \quad \forall v \in H^1(\Omega). \tag{13}$$

Where, $\forall u, v \in H^1(\Omega)$

$$\begin{aligned} a(u,v) &= \int_\Omega \nabla u \, \nabla \bar{v} \, dx + \alpha \int_\Omega u \, \bar{v} \, dx + i \int_{\partial\Omega} u \, \bar{v} \, d\sigma, \\ l(v) &= \int_\omega h_1 \, \bar{v} \, dx + \int_{\Omega \setminus \overline{\omega}} h_2 \, \bar{v} \, dx + \int_{\partial\Omega} g \, \bar{v} \, d\sigma + i \int_{\partial\Omega} f \, \bar{v} \, d\sigma. \end{aligned}$$

We show a well-posedness result of the complex boundary value problem (7) in the following proposition

Proposition 3.1. *For a given $\omega \in \Omega_\delta$, the complex boundary value problem (7) has a unique stable weak solution in $H^1(\Omega)$ satisfying*

$$\|u\|_{1,\Omega} \leq C \left(\|f\|_{0,\partial\Omega} + \|g\|_{0,\partial\Omega} + \|h_1\|_{0,\Omega} + \|h_2\|_{0,\Omega} \right).$$

Proof. We apply the complex version of Lax-Milgram Lemma by showing that the sesquilinear form $a(.,.)$ (*i.e.*, $u \mapsto a(u,v)$ is linear, and $v \mapsto a(u,v)$ is anti-linear) is continuous on $H^1(\Omega) \times H^1(\Omega)$ (*i.e.*, $\exists c > 0$, $|a(u,v)| \leq c\|u\|_{1,\Omega}\|v\|_{1,\Omega}$, $\forall (u,v) \in H^1(\Omega) \times H^1(\Omega)$) and H^1-coercive (*i.e.*, $\exists c > 0$, $Re\ a(u,u) \geq c\|u\|^2_{1,\Omega}$, $\forall u \in H^1(\Omega)$), and the linear form $l(.)$ is continuous on $H^1(\Omega)$ (*i.e.*, $\exists c > 0$, $|l(v) \leq c\|v\|_{1,\Omega}$, $\forall v \in H^1(\Omega)$).
For any $u, v \in H^1(\Omega)$ we have

$$Re\ a(u,u) = \int_\Omega |\nabla u|^2 dx + \alpha \int_\Omega |u|^2 dx \geq min(1,\alpha)\|u\|^2_{1,\Omega}$$

Hölder and the trace inequalities imply that

$$\begin{aligned} |a(u,v)| &\leq |\int_\Omega \nabla u \, \nabla \bar{v} \, dx| + \alpha |\int_\Omega u \, \bar{v} \, dx| + |\int_{\partial\Omega} u \, \bar{v} \, d\sigma| \\ &\leq \|\nabla u\|_{0,\Omega}\|\nabla v\|_{0,\Omega} + \alpha\|u\|_{0,\Omega}\|v\|_{0,\Omega} + \|u\|_{0,\partial\Omega}\|v\|_{0,\partial\Omega} \\ &\leq \|u\|_{1,\Omega}\|v\|_{1,\Omega} + \alpha\|u\|_{1,\Omega}\|v\|_{1,\Omega} + c^2\|u\|_{1,\Omega}\|v\|_{1,\Omega} \\ &\leq \left(1 + \alpha + c^2\right) \|u\|_{1,\Omega}\|v\|_{1,\Omega} \end{aligned}$$

Finally, the continuity of the linear form $l(.)$ can be proved similarly. We have

$$\begin{aligned} |l(v)| &\leq |\int_\Omega \chi_\omega \, h_1 \, \bar{v} \, dx| + |\int_\Omega \chi_{\Omega\setminus\overline{\omega}} \, h_2 \, \bar{v} \, dx| + |\int_{\partial\Omega} g \, \bar{v} \, d\sigma| + |\int_{\partial\Omega} f \, \bar{v} \, d\sigma| \\ &\leq \|h_1\|_{0,\Omega}\|v\|_{0,\Omega} + \|h_2\|_{0,\Omega}\|v\|_{0,\Omega} + \|g\|_{0,\partial\Omega}\|v\|_{0,\partial\Omega} + \|f\|_{0,\partial\Omega}\|v\|_{0,\partial\Omega} \\ &\leq \left(\|h_1\|_{0,\Omega} + \|h_2\|_{0,\Omega} + c\|g\|_{0,\partial\Omega} + c\|f\|_{0,\partial\Omega}\right) \|v\|_{1,\Omega} \end{aligned}$$

where c is a constant from the trace inequality. By the complex version of Lax-Milgram Lemma ([11], page 368), Problem (7) admits a unique solution $u \in H^1(\Omega)$ which depends continuously on data. Moreover,

$$\beta\|u\|^2_{1,\Omega} \leq Re\ a(u,u) \leq |a(u,u)| = |l(u)| \leq \gamma\|u\|_{1,\Omega}$$

where $\beta = min(1,\alpha)$, and $\gamma = \|h_1\|_{0,\Omega} + \|h_2\|_{0,\Omega} + c\|g\|_{0,\partial\Omega} + c\|f\|_{0,\partial\Omega}$.
Then

$$\|u\|_{1,\Omega} \leq \frac{\gamma}{\beta}. \tag{14}$$

□

4. Existence of an optimal solution

The existence of optimal shape requires some continuity or at least lower semicontinuity of the functional to be minimized. This also implies having continuity of the solution of the associated partial differential equation with respect to the variations of the domain in an adequate topology. In this section, we analyze in detail the continuity of the shape functional and the mapping $\omega \to u_\omega \in H^1(\Omega)$, where u_ω is the solution of the complex problem (7) corresponding to a variable open subset ω of the fixed open set Ω_δ.

It is necessary to add extra conditions on the variable domains to expect good convergence of the solutions. We state a classical sufficient condition, in terms of uniform regularity of the domains, the $\varepsilon-$cone property, and we define the family of admissible domains

$$\mathcal{O} = \{\omega \subset \Omega_\delta,\ \omega \text{ open with the } \varepsilon\text{-cone property}\}. \tag{15}$$

Proposition 4.1. *There exists $\omega \in \mathcal{O}$ such that*

$$J(\omega) = \inf\{J(\omega^*),\ \ \omega^* \in \mathcal{O}\}.$$

Proof. Let $(\omega_n)_n \subset \mathcal{O}$ be a minimizing sequence such that $J(\omega_n) \longrightarrow \inf J(\omega)$. Since $\mathcal{O}$ is compact for the topology of characteristic functions (see [25], page 59), then there exist an open set $\omega \subset \mathcal{O}$ and a subsequence denoted also $(\omega_n)_n \subset \mathcal{O}$ that converges to ω in the sense of characteristic functions.
We denote by u_n, u the solutions of the complex problem (7) corresponding respectively to ω_n, ω. From (14) we have, $\forall n \quad \|u_n\|_{1,\Omega} \leq \dfrac{\gamma}{\beta}$.
This shows that the sequence u_n is bounded in $H^1(\Omega)$. Up to a subsequence, it may be assumed that u_n converges weakly in $H^1(\Omega)$ and strongly in $L^2(\Omega)$ to a function $u^* \in H^1(\Omega)$. Let us show that u^* satisfies the variational formulation of problem (7) corresponding to ω.
By definition of u_n, for all $v \in H^1(\Omega)$,

$$\int_\Omega \nabla u_n\, \nabla \bar{v} + \alpha \int_\Omega u_n\, \bar{v} + i \int_{\partial\Omega} u_n\, \bar{v} = \int_{\omega_n} h_1\, \bar{v} + \int_{\Omega\setminus\overline{\omega}_n} h_2\, \bar{v} + \int_{\partial\Omega} g\, \bar{v} + i \int_{\partial\Omega} f\, \bar{v} \tag{16}$$

Since $\chi_{\omega_n} \to \chi_\omega$ weakly * in $L^\infty(\Omega)$, $p\, v \in L^1(\Omega)$ then

$$\int_\Omega \chi_{\omega_n} h_1\, \bar{v} \to \int_\Omega \chi_\omega h_1\, \bar{v} \quad \text{and} \quad \int_\Omega \chi_{\Omega\setminus\overline{\omega}_n} h_2\, \bar{v} \to \int_\Omega \chi_{\Omega\setminus\overline{\omega}}\, h_2\, \bar{v}.$$

We know that $u_n \rightharpoonup u^*$ in $H^1(\Omega)$, then $\nabla u_n \rightharpoonup \nabla u^*$ in $L^2(\Omega)$, we get

$$\int_\Omega \nabla u_n \nabla \bar{v} \to \int_\Omega \nabla u^* \nabla \bar{v}$$

We have $u_n \to u^*$ in $L^2(\Omega)$, it follows that

$$\int_\Omega u_n \bar{v} \to \int_\Omega u^* \bar{v}.$$

By compacity of the trace from $H^1(\Omega)$ to $L^2(\partial\Omega)$, we can extract a subsequence $u_n \to u^*$ in $L^2(\partial\Omega)$, we deduce that

$$\int_{\partial\Omega} u_n \bar{v} \to \int_{\partial\Omega} u^* \bar{v}.$$

Therefore, for all $v \in H^1(\Omega)$,

$$\int_\Omega \nabla u^* \nabla \bar{v} + \alpha \int_\Omega u^* \bar{v} + i \int_{\partial\Omega} u^* \bar{v} = \int_\omega h_1\, \bar{v} + \int_{\Omega\setminus\overline{\omega}} h_2\, \bar{v} + \int_{\partial\Omega} g\, \bar{v} + i \int_{\partial\Omega} f\, \bar{v} \tag{17}$$

This proves that $u^* = u(\omega)$.
Let us denote by u_2^n the imaginary part of u_n, and u_2 the imaginary part of u. We have $\|u_n\|_{0,\Omega} \longrightarrow \|u\|_{0,\Omega}$, and therefore

$$\|u_2^n\|_{0,\Omega} \longrightarrow \|u_2\|_{0,\Omega}.$$

Since the perimeter is lower semicontinuous with respect to the convergence of characteristic functions (see [25], page 51),

$$P_\Omega(\omega) \leq \liminf P_\Omega(\omega_n). \tag{18}$$

We can infer that

$$J(\omega) \leq \liminf J(\omega_n).$$

Which implies that ω is a minimizer of (11). □

5. Shape derivative calculus

In order to use a descent method of gradient type, it is necessary to differentiate the shape functional J with respect to the shape variable ω. To define the shape derivative, we will use the so called velocity method, which is, for instance, introduced in [23]. To this end, we consider the variation of a given smooth reference shape ω according to the displacement V, defined by $\phi_t(x) = x + tV(x)$, where V a smooth vector field with compact support in Ω_δ, and we denote by $\mathcal{V}$ the space of admissible deformations V. It is well known that ϕ is invertible, for sufficiently small t.

We say that the functional $J(\omega)$ has an Eulerian derivative at ω in the direction V if the limit

$$\lim_{t\to 0} \frac{J(\phi_t(\omega)) - J(\omega)}{t} := DJ(\omega).V$$

exists. Furthermore, if the mapping $V \longmapsto DJ(\omega).V = \langle \nabla J, V\rangle$ is linear and continuous, we say that J is shape differentiable at ω. When J has an Eulerian derivative, we say that ∇J is the shape gradient of J at ω. For more details concerning the differentiation with respect to the domain, we refer to the books [12, 18, 25].

5.1. Shape gradient of the cost function

Computing the shape gradient of the cost functional requires to calculate also the shape derivative of the state (7). Numericaly, it implies that we need to solve as many boundary problems as discrete shape variables. To avoid this extra computational cost, we use the classical adjoint state method, which requires to solve only one extra boundary value problem.

By introducing the suitable adjoint problem, we give the shape gradient of the cost function in the following proposition.

Proposition 5.1. *Let $V \in \mathcal{V}$, the cost functional J is differentiable with respect to the shape ω in the direction of V and its shape derivative is given by*

$$DJ(\omega).V = \int_{\partial\omega} (q_2(h_2 - h_1) + \varepsilon\kappa)V_n, \tag{19}$$

where $\kappa = div_\Gamma(n)$, and $q = q_1 + iq_2$ solves the following adjoint problem

$$\begin{cases} -\Delta q + \alpha q = u_2 \text{ in } \Omega, \\ \partial_n q - iq = 0 \text{ on } \partial\Omega. \end{cases} \tag{20}$$

Proof. First, we derive the following expression using Hadamard and divergence formulas

$$\begin{aligned} DJ(\omega).V &= \int_\Omega u_2 u_2' + \frac{1}{2}\int_\Omega div(|u|^2 V) + \varepsilon \int_{\partial\omega} div_\Gamma(V) \\ &= \int_\Omega u_2 u_2' + \frac{1}{2}\int_{\partial\Omega} |u|^2 V_n + \varepsilon \int_{\partial\omega} div_\Gamma(V_n n) \\ &= \int_\Omega u_2 u_2' + \varepsilon \int_{\partial\omega} V_n div_\Gamma(n). \end{aligned}$$

Where div_Γ denotes the tangential divergence on $\partial\omega$, and κ is the mean curvature of $\partial\omega$.
On the other hand, one can show that the shape derivative of the state solves the following boundary value problem (see Appendix)

$$\begin{cases} \Delta u' + \alpha u' = 0 & \text{in } \Omega, \\ [u'] = 0 & \text{on } \partial\omega, \\ [\partial_n u'] = (h_1 - h_2) V_n & \text{on } \partial\omega, \\ \partial_n u' + i u' = 0 & \text{on } \partial\Omega. \end{cases} \tag{21}$$

Then, the weak formulation of (21) with q the solution of (20) as a test function, and the weak formulation of (20) with u' as a test function, are given by

$$\int_\Omega \nabla u' \nabla \bar{q} + \alpha \int_\Omega u' \bar{q} + i \int_{\partial\Omega} u' \bar{q} = \int_{\partial\omega} (h_1 - h_2) \bar{q} V_n, \tag{22}$$

$$\int_\Omega \nabla q \nabla \bar{u}' + \alpha \int_\Omega q \bar{u}' - i \int_{\partial\Omega} q \bar{u}' = \int_\Omega u_2 \bar{u}', \tag{23}$$

(23) implies that

$$\int_\Omega \nabla u' \nabla \bar{q} + \alpha \int_\Omega u' \bar{q} + i \int_{\partial\Omega} u' \bar{q} = \int_\Omega u_2 u', \tag{24}$$

By (22) and (24), it follows

$$\int_\Omega u_2 u' = \int_{\partial\omega} (h_1 - h_2) \bar{q} V_n.$$

Finally, we conclude that

$$\int_\Omega u_2 u_2' = -\int_{\partial\omega} q_2 (h_1 - h_2) V_n.$$

□

6. Algorithm and numerical results

In this section, we present some numerical simulations in order to confirm and complete our previous theoretical results with a comparison between CCBM, Least-squares and Kohn-Vogelius Methods. In order to solve numerically the optimization problem (12), we opt for the classical shape variation descent algorithm. First of all, we describe the algorithm and the framework used, then, we present the numerical simulations and some comparisons.

6.1. Algorithm

The shape derivative of the cost function J along a deformation field V can be expressed as

$$\nabla J(\omega)[V] = \int_{\partial\omega} RV_n d\sigma,$$

where $R = q_2(h_2 - h_1) + \varepsilon\kappa$ where q_2 is the imaginary part of q the solution of the adjoint problem (20). The deformation field V is chosen to provide a descent direction of the cost function $J(\omega)$, thus $V = -R.n$ on $\partial\omega$ is a descent direction. In addition, it is well known that the shape gradient is defined on the boundary of the moving shape [28], using this approach, the direction of descent must be defined only on $\partial\omega$. However, if the boundary measurements (f, g) is not sufficiently smooth, the surface expression of the shape gradient may not exist or the direction of descent V may have a poor regularity. Therefore, it is interesting to derive a direction of descent V on Ω from the volumetric expression of the shape gradient. Which requires solving another additional variational problem. Let V be the Riesz representative of $-\nabla J(\omega)$, *i.e.* (see [7] and [16])

$$< V, \phi >_{H^1(\Omega)} = -\nabla J(\omega)[\phi] = - < R.n, \phi >_{L^2(\partial\omega)} \quad \forall \phi \in D^2, \tag{25}$$

where

$$D = \Big\{ \phi \in H^1(\Omega), \quad \phi = 0 \ \ in \quad \partial\Omega \Big\},$$

and $<,>$ is the inner product on D^2 defined by

$$< V, \phi >_{H^1(\Omega)} = \int_\Omega \nabla V : \nabla\phi + V.\phi.$$

The equation (25) is the week formulation for the following system

$$\begin{cases} -\Delta V + V = & 0 & \text{in} & \Omega, \\ V = & 0 & \text{on} & \partial\Omega, \\ [\partial_n V] = & -R.n & \text{on} & \partial\omega. \end{cases} \tag{26}$$

We give in the following algorithm the gradient method of our problem.

Algorithm 1: Gradient algorithm for shape optimization

1: Choose an initial shape ω_0, set $k = 0$ and iterate:
2: Solve the state problem (7) and the adjoint problem (20) for $\omega = \omega_k$.
3: Compute the descent direction V_k using (26).
4: Update the current boundary $\partial\omega_k$ by V_k to obtain $\partial\omega_{k+1}$, *i.e.*, set $\partial\omega_{k+1} := \{x + t_k V_k(x) : \quad x \in \partial\omega_k\}$, for some sufficiently small scalar $t_k > 0$.
5: While $\|\nabla J(\omega_k).V_k\| \geq \epsilon$, $\quad k = k + 1$ and repeat .

6.2. Numerical results

For the numerical simulations, we consider the dimension two and we use the finite elements Software Freefem++ (see [19]). The exterior boundary $\partial\Omega$ is assumed to be the square $[-1, 1] \times [-1, 1]$. We construct the synthetic data on $\partial\Omega$, by fixing the shape ω and choosing the Neumann boundary condition $g(t) = \sin(t)$, $t \in [0, 2\pi]$, then, we compute the trace of state u solution of (4) to extract the measurement $f = u \quad on \quad \partial\Omega$. For the latter equation, we use a P_2 finite elements discretization to solve the direct problem. The examples with noisy data are generated by perturbing the Dirichlet data f using a fixed amplitude of

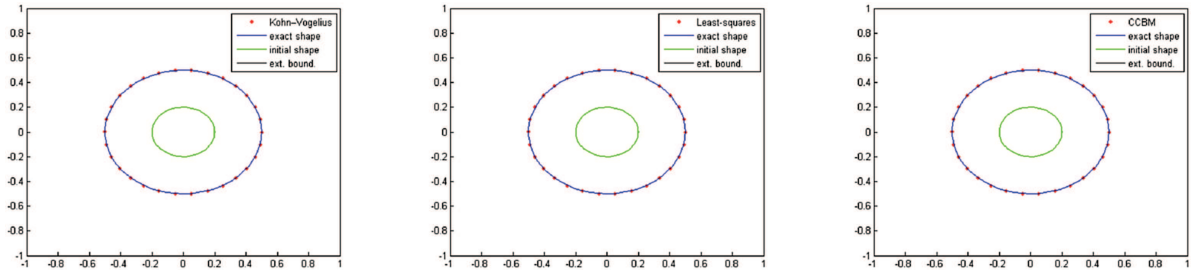

(a) (b) (c)

FIGURE 1. Reconstruction of the first domain by Kohn-Vogelius, Least-squares and CCBM methods. (a) Kohn-Vogelius. (b) Least-squares. (c) CCBM.

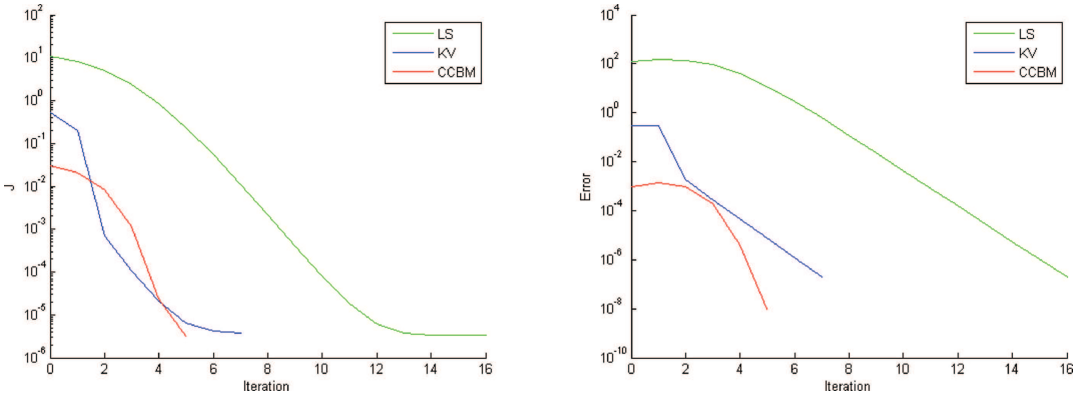

(a) (b)

FIGURE 2. Evolution of the three cost functions and their gradients according to the number of iterations. (a) Cost functions. (b) Gradients.

Gaussian noise. The synthetic data has been chosen, in a way to avoid the so-called inverse crime phenomena. To this end, the size of discretization used to obtain the synthetic data is different from the one used for solving the inverse problem.

We precise that in all tests, the exterior boundary is represented by the black line, the initial shape by the green line, the exact shape to identify by the blue line and the reconstructed shape by the dotted red line.

6.2.1. Results without noise

we present in Figures 1 and 3, the reconstruction result by three cost functionals, in the left, the identification by the Kohn-Vogelius cost function, in the middle the Least-squares, and in the right, the result obtained by CCBM. we notice that the results obtained are effective and similar.

In Figures 2 and 4, we plot the variation of the cost functionals according to the number of iterations and the evolution of their associated gradients also. Clearly, The CCBM converges much quicker than the two other methods.

In Figures 5 and 7, we observe that the results obtained by the CCBM and Kohn-Vogelius is more robust than those obtained by Least-squares. In Figures 6 and 8, the convergence of the CCBM dominates that of the Kohn-Vogelius and Least-squares.

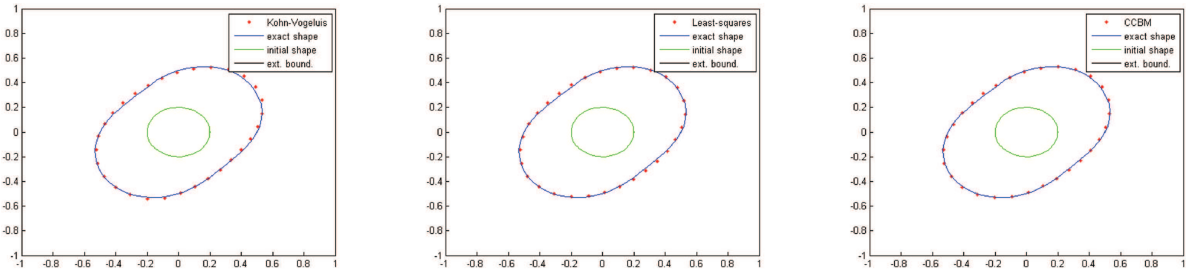

(a) (b) (c)

FIGURE 3. Reconstruction of the unknown domain by the three methods. (a) Kohn-Vogelius. (b) Least-squares. (c) CCBM.

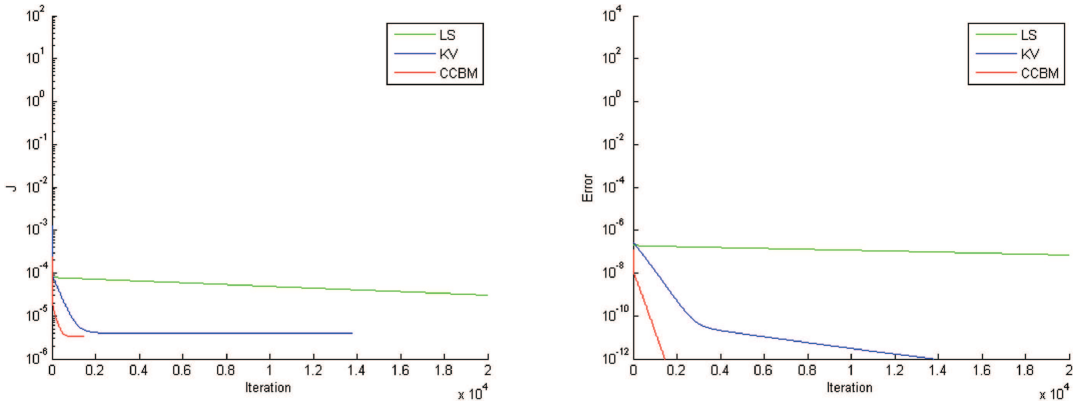

(a) (b)

FIGURE 4. Evolution of the three cost functions, and their associated gradients according to the number of iterations. (a) Cost functions. (b) Gradients.

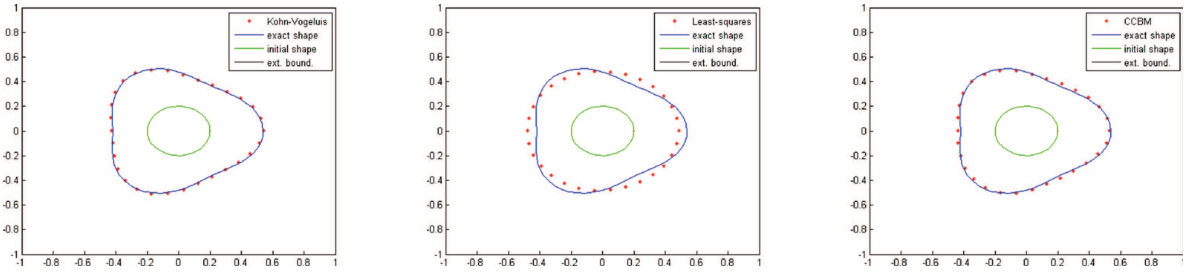

(a) (b) (c)

FIGURE 5. Reconstruction of the unknown domain by the three methods methods. (a) Kohn-Vogelius. (b) Least squares. (c) CCB.

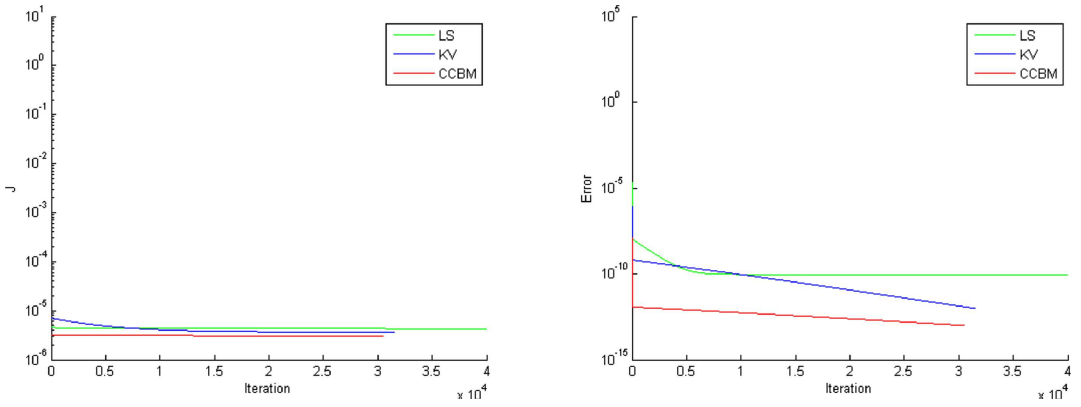

(a) (b)

FIGURE 6. Evolution of the three cost functions and their gradients according to the number of iterations. (a) Cost functions. (b) Gradients.

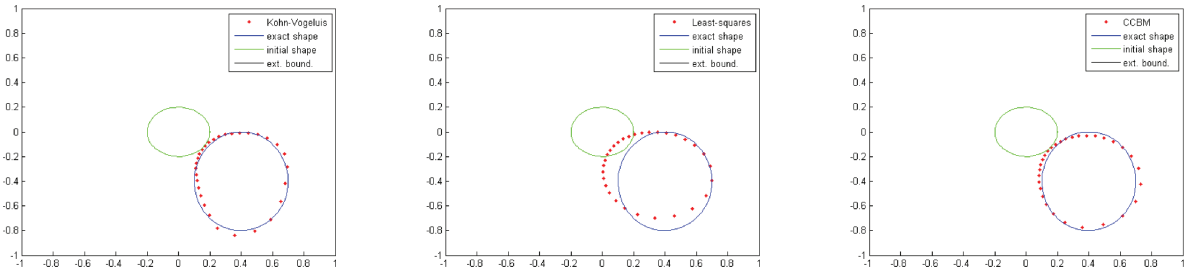

(a) (b) (c)

FIGURE 7. Reconstruction of the unknown domain by three methods. (a) Kohn-Vogelius. (b) Least squares. (c) CCBM.

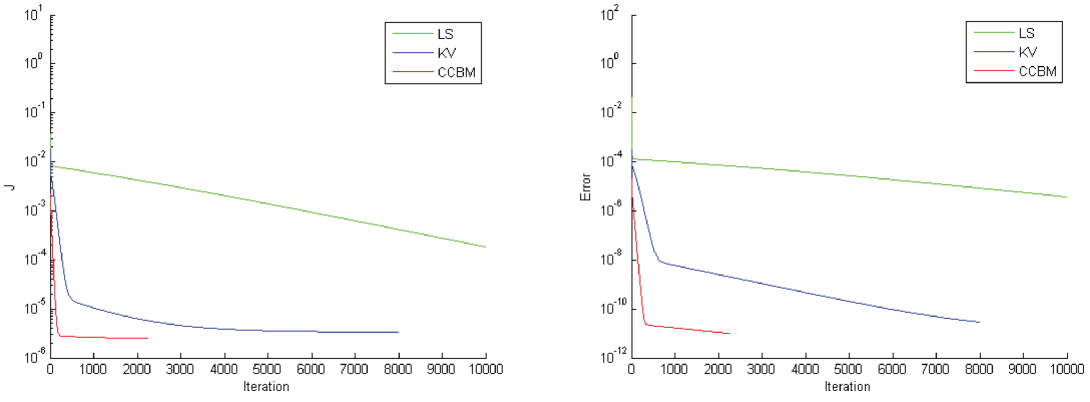

(a) (b)

FIGURE 8. Evolution of the three cost functions and their gradients according to the number of iterations. (a) Cost functions. (b) Gradients.

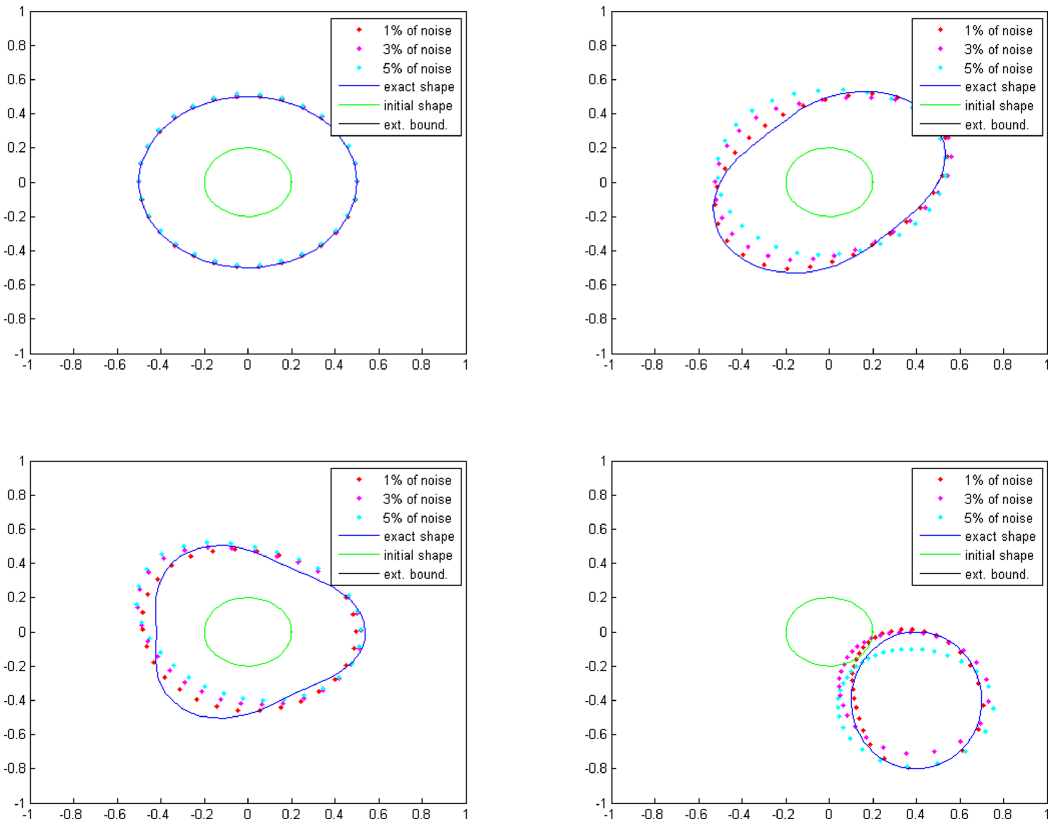

FIGURE 9. Reconstructions of the unknown domain with noise.

6.2.2. Results with Gaussian noise

In this subsection, we present the results obtained from the noisy data as follows

$$\tilde{f}(x) = f(x)\big(1 + \tau\xi\big),$$

where ξ is a uniformly distributed random variable in $[-1, 1]$ and τ dictates the level of noise.
We present in Figure 9, the results with different levels of noise. We observe that for different geometries the CCBM gives good results.

6.2.3. Results with impulse noise

Having shown the stability of the proposed method with noised data infected with Gaussian noise, we present in this section the robustness of this method through a more complicated type of noise. We suppose that the given data is infected by the impulse noise. Impulse noise consists of relatively short duration "on/off" noise pulses, caused by a variety of sources, dropouts, or surface degradation. The impulse noise is not trivial due to its complex statistical nature. To construct noised data, we select randomly a number of nodes in the boundary $\partial\Omega$ with a percentage ϱ. Then we add the impulsive noise to data as follows:

$$f_\varrho = f_\varrho + \varrho\eta\iota\|f_\varrho\|_\infty$$

where η is the magnitude of corruption, $\|f_\varrho \cdot\|_\infty$ is the maximum norm. While ι is a vector of impulsive noise which have the following probability density function

$$\mathfrak{D}(\iota_i(x)) = \lambda_1\delta(\iota_i(x)) + \lambda_2\mathfrak{D}_N(\iota_i(x))$$

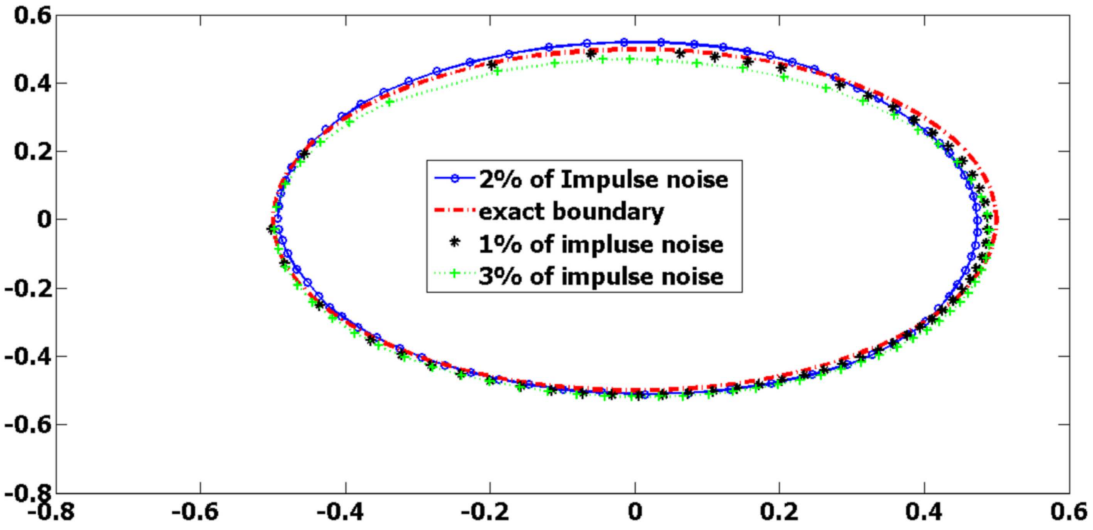

FIGURE 10. Plot of different boundaries obtained with noised data with different rates of impulsive noise.

where $\delta(\iota_i(x))$ is the Kronecker delta function and $\mathfrak{D}_N(\iota_i(x))$ is a zero-mean Gaussian probability density function. While λ_1 and λ_2 are parameters that control the mixture of a discrete probability mass function $\delta(\iota_i(x))$ and a continuous probability density function.

In Figure 10, we present the plot of different obtained boundaries by the algorithm 1, using data with different rates of impulsive noise. For the case of 1% rate of impulsive noise, the percentage of corrupted data points is $\varrho = 30\%$ and the magnitude of corruption is $\eta = 0.1$. In the case of 2% rate of impulsive noise, we have taken $\varrho = 50\%$ as percentage of corrupted data points and $\eta = 0.2$ as magnitude of corruption. While in the last case, all nodes of boundary $\partial\Omega$ was affected by noise which corresponds to $\varrho = 100\%$ and the magnitude of corruption was $\eta = 0.5$. As we can see in this case of more complicated noise, the proposed approach still present a good approximation which prove numerically its stability.

6.2.4. Real case without exact solution

In this section we consider a case with data from real life situation. We consider an electrostatic problem. We consider a rectangular domain $\Omega =]-1, 1[^2$. Denote by Ψ the source term of electrostatic charges which supposed discontinued through the inclusion ω and let (g, f) be given data on the boundary. Our goal is to reconstruct surface charges ω that creating the potential field u from Cauchy data (g, f). The Cauchy data are taken as follows : the measured potential f on the boundary is presented in the Figure 11. the output flux $g = 0$. While the source $h_1 = 12v$ and $h_2 = 230v$. The mesh of the optimal domain is presented in the Figure 12. In the Figure 13, we present the evolution of the cost functional J and the norm of the gradient $|\nabla J|$ according to iterations. In the Figure 14, we present the potential in optimal domain for 2 and 3 dimensions.

As we can be seen, the obtained results in the real-life case show the performance of the proposed approach.

7. CONCLUSION

We have presented a regularized Complex coupled formulation for the identification of the geometric source problem. The inverse problem is reformulated as a shape optimization one. The existence of a minimizer is investigated. A numerical algorithm for solving the proposed optimization problem is developed. We also derived an exact computation of the gradient of the cost function of our optimization problem. The numerical experiments

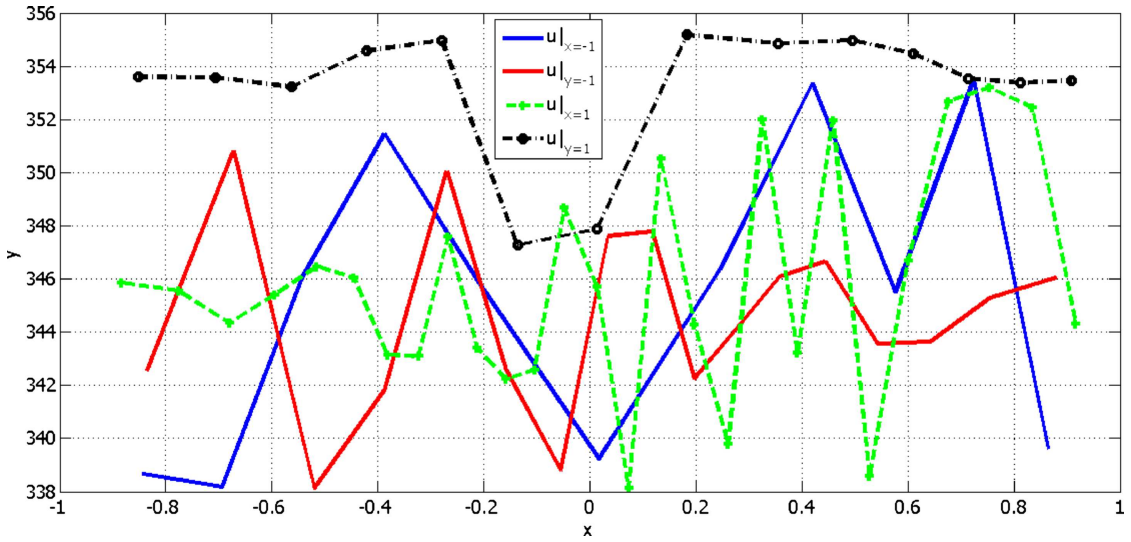

FIGURE 11. The measured potential on different parts of the boundary $\partial\Omega$.

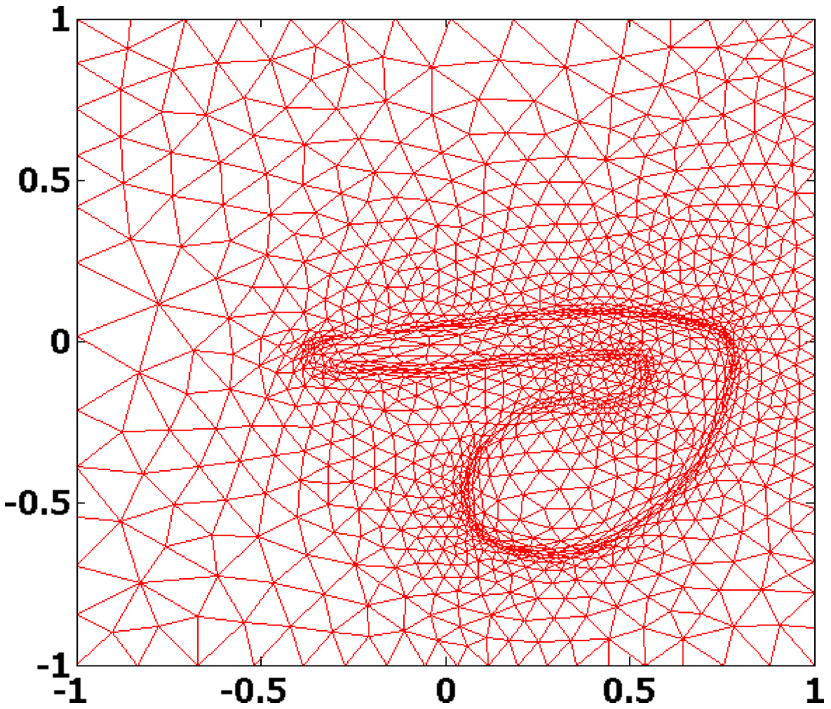

FIGURE 12. The mesh of the optimal configuration of domain showing the inclusion ω.

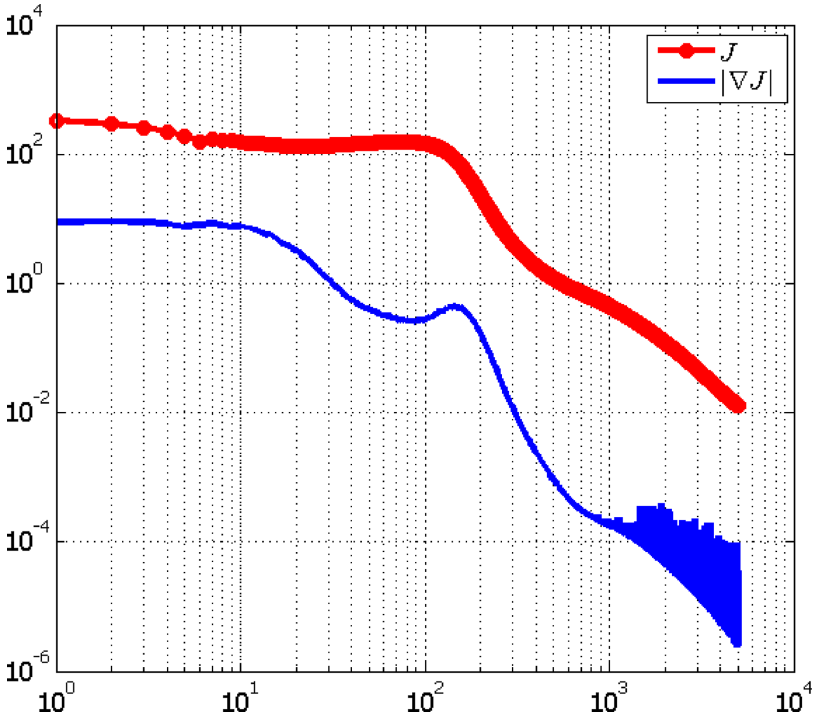

FIGURE 13. The evolution of the cost function and the norm of the gradient.

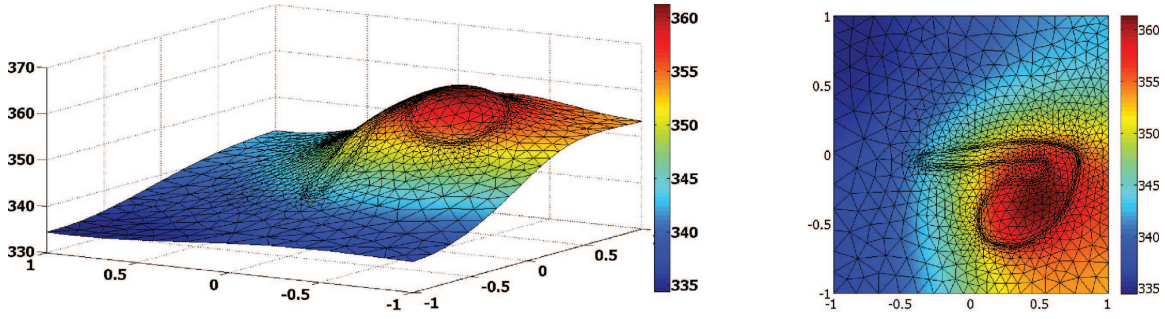

(a) (b)

FIGURE 14. The plot of the optimal potential in 2 dimensions and 3 dimensions.

performed in this paper demonstrate the robustness of the developed regularized coupled method for solving this geometric inverse problems.

APPENDIX A. SHAPE DERIVATIVE OF THE STATE

Before starting, we give some notations. We denote by n the outward unit normal to $\partial\omega$ pointing into $\Omega \setminus \overline{\omega}$, thus $\partial_n u^-$ (resp. $\partial_n u^+$) is the normal derivative from the inside of ω (resp. $\Omega \setminus \overline{\omega}$) at interface $\partial\omega$, and $[\cdot]$ denotes the jump across the same interface. Let $V \in \mathcal{V}$ and $V_n := \langle V, n \rangle$ its normal component. Consider the smooth

transformation $\phi_t(x) = x + tV(x)$. We denote by

$$\begin{aligned} J_t(x) &= \det D\phi_t(x), \\ A_t(x) &= D\phi_t^{-1}(x)^\intercal D\phi_t^{-1}(x) J_t(x), \\ \xi_t(x) &= J_t(x) \| D\phi_t^{-T}(x).n \|. \end{aligned}$$

Note that $A_t(x)$ is symmetric positive and for $t < t_0$ we have

$$y^\intercal A_t(x) y \geq \mu \|y\|^2 \quad \text{and} \quad 0 < \beta \leq J_t.$$

Furthermore, the application A_t is smooth with $A_0(x) = I$, $J_0(x) = 1$ and

$$\mathcal{A} := \begin{aligned} \frac{d}{dt} J_t(x)_{|t=0} &= \operatorname{div}(V), \\ \frac{d}{dt} A_t(x)_{|t=0} &= \operatorname{div}(V) I - (DV^\intercal + DV), \\ \frac{d}{dt} \xi_t(x)_{|t=0} &= \operatorname{div}(V) - \langle DV.n, n \rangle = div_\Gamma(V). \end{aligned}$$

We denote by u_t the solution of (7) with inclusion $\omega_t = \phi_t(\omega)$. For the computation of the shape gradient of the state, we shall use the classical technique which consists of transporting the quantity u_t defined in the variable domain ω_t back onto the reference domain ω using the following transformation $u^t = u_t \circ \phi_t$, the usual methods of differential calculus can now be applied since both functionals u^t and u are now defined in the fixed domain ω. The material derivative (or Lagrangian derivative) of the state is then given by

$$\dot{u} := \lim_{t \to 0} \frac{u^t - u}{t}, \quad \forall x \in \Omega.$$

The shape derivative (or Eulerian derivative) of the state is defined by

$$u' := \dot{u} - \nabla u.V.$$

Theorem A.1. *The state solution u has a material derivative $\dot{u}$ that satisfies*

$$\begin{aligned} \forall v \in H^1(\Omega), \quad \langle \nabla \dot{u}, \nabla v \rangle_{0,\Omega} + \alpha \langle \dot{u}, v \rangle_{0,\Omega} = &- \langle \mathcal{A} \nabla u, \nabla v \rangle_{0,\Omega} - \alpha \langle \operatorname{div}(V) u, v \rangle_{0,\Omega} + \langle \operatorname{div}(V) h_2, v \rangle_{0,\Omega} \\ &+ \langle \nabla h_2.V, v \rangle_{0,\Omega} + \langle \operatorname{div}(V)(h_1 - h_2), v \rangle_{0,\omega} \\ &+ \langle \nabla (h_1 - h_2).V, v \rangle_{0,\omega}. \end{aligned} \tag{A.1}$$

The state u is shape differentiable and its shape derivative u' solves

$$\begin{cases} \Delta u' + \alpha u' = 0 & \text{in } \Omega, \\ [u'] = 0 & \text{on } \partial\omega, \\ [\partial_n u'] = (h_1 - h_2) V_n & \text{on } \partial\omega, \\ \partial_n u' + i u' = 0 & \text{on } \partial\Omega. \end{cases} \tag{A.2}$$

We think it is useful to show how, using the classical methods of shape optimization, we can prove both existence of the derivative and problem (A.2). Therefore, we give a rigorous proof of Theorem A.1 and also show that material derivative is belonging to $H^1(\Omega)$.

Proof. The proof is divided into four parts. Firstly, we transfer the perturbed problem to the fixed domain, we then prove weak convergence of a given sequence to the material derivative of the state, next, we show its stong convergence, and finally, we deduce the shape derivative.

First step. Let u_t denote the solution of Problem (7) given in a domain with inclusion $\omega_t = \phi_t(\omega)$, we have

$$\forall v \in H^1(\Omega), \quad \int_\Omega \nabla u_t.\nabla \bar{v} + \alpha \int_\Omega u_t \bar{v} + i \int_{\partial\Omega} u_t \bar{v} = \int_\Omega h_2 \bar{v} + \int_{\omega_t} (h_1 - h_2)\bar{v} + \int_{\partial\Omega} g\bar{v} + i \int_{\partial\Omega} f\bar{v}.$$

Then, the transported $u^t = u_t \circ \phi_t$ solves the variational equation

$$\int_\Omega A_t \nabla u^t.\nabla \bar{v} + \alpha \int_\Omega u^t \bar{v} J_t + i \int_{\partial\Omega} u^t \bar{v} = \int_\Omega h_2 \circ \phi_t \bar{v} J_t + \int_\omega (h_1 \circ \phi_t - h_2 \circ \phi_t)\bar{v} J_t + \int_{\partial\Omega} g\bar{v} + i \int_{\partial\Omega} f\bar{v}. \quad \text{(A.3)}$$

Second step. Using the variational equation solved by u subtracted from the equation (A.3), and the fact that $\phi_t(x) = x$ on $\partial\Omega$, we obtain

$$\begin{aligned} \Big\langle A_t \frac{\nabla u^t - \nabla u}{t}, \nabla v \Big\rangle_{0,\Omega} + \alpha \Big\langle J_t \frac{u^t - u}{t}, v \Big\rangle_{0,\Omega} &= \Big\langle \frac{I - A_t}{t} \nabla u, \nabla v \Big\rangle_{0,\Omega} + \alpha \Big\langle \frac{1 - J_t}{t} u, v \Big\rangle_{0,\Omega} \\ &+ \Big\langle J_t \frac{h_2 \circ \phi_t - h_2}{t}, v \Big\rangle_{0,\Omega} + \Big\langle \frac{J_t - 1}{t} h_2, v \Big\rangle_{0,\Omega} \\ &+ \Big\langle J_t \frac{(h_1 \circ \phi_t - h_2 \circ \phi_t) - (h_1 - h_2)}{t}, v \Big\rangle_{0,\omega} \\ &+ \Big\langle \frac{J_t - 1}{t}(h_1 - h_2), v \Big\rangle_{0,\omega}. \end{aligned} \quad \text{(A.4)}$$

Using $\dfrac{(u^t - u)}{t}$ as a test function, and from the properties of A_t and J_t we get

$$\begin{aligned} \mu \Big\| \frac{\nabla u^t - \nabla u}{t} \Big\|^2_{0,\Omega} + \beta\alpha \Big\| \frac{u^t - u}{t} \Big\|^2_{0,\Omega} &\le \Big\| \frac{A_t - I}{t} \Big\|_\infty \Big\| \nabla u \Big\|_{0,\Omega} \Big\| \frac{\nabla u^t - \nabla u}{t} \Big\|_{0,\Omega} + \alpha \Big\| \frac{1 - J_t}{t} \Big\|_\infty \Big\| u \Big\|_{0,\Omega} \Big\| \frac{u^t - u}{t} \Big\|_{0,\Omega} \\ &+ \Big\| J_t \Big\|_\infty \Big\| \frac{h_2 \circ \phi_t - h_2}{t} \Big\|_{0,\Omega} \Big\| \frac{u^t - u}{t} \Big\|_{0,\Omega} + \Big\| \frac{J_t - 1}{t} \Big\|_\infty \Big\| h_2 \Big\|_{0,\Omega} \Big\| \frac{u^t - u}{t} \Big\|_{0,\Omega} \\ &+ \Big\| J_t \Big\|_\infty \Big\| \frac{(h_1 \circ \phi_t - h1) - (h_2 \circ \phi_t - h_2)}{t} \Big\|_{0,\Omega} \Big\| \frac{u^t - u}{t} \Big\|_{0,\Omega} \mathrm{mes}(\Omega_\delta)^{1/2} \\ &+ \Big\| \frac{J_t - 1}{t} \Big\|_\infty \Big\| h_1 - h_2 \Big\|_{0,\Omega} \Big\| \frac{u^t - u}{t} \Big\|_{0,\Omega} \mathrm{mes}(\Omega_\delta)^{1/2}. \end{aligned}$$

From Young's inequality, we deduce that

$$\begin{aligned} min(\mu, \beta\alpha) \Big\| \frac{u^t - u}{t} \Big\|_{0,\Omega} \le C \Bigg(& \Big\| \frac{A_t - I}{t} \Big\|_\infty \Big\| \nabla u \Big\|_{0,\Omega} + \alpha \Big\| \frac{1 - J_t}{t} \Big\|_\infty \Big\| u \Big\|_{0,\Omega} + \Big\| J_t \Big\|_\infty \Big\| \frac{h_2 \circ \phi_t - h_2}{t} \Big\|_{0,\Omega} \\ & + \Big\| \frac{J_t - 1}{t} \Big\|_\infty \Big\| h_2 \Big\|_{0,\Omega} + \Big\| J_t \Big\|_\infty \Big\| \frac{(h_1 \circ \phi_t - h1) - (h_2 \circ \phi_t - h_2)}{t} \Big\|_{0,\Omega} \mathrm{mes}(\Omega_\delta)^{1/2} \\ & + \Big\| \frac{J_t - 1}{t} \Big\|_\infty \Big\| h_1 - h_2 \Big\|_{0,\Omega} \mathrm{mes}(\Omega_\delta)^{1/2} \Bigg), \end{aligned}$$

where C is a positive constant. Therefore the sequence $(u^t - u)/t$ is bounded in $H^1(\Omega)$. Thus, we obtain the weak convergence of the sequence in $H^1(\Omega)$ and its weak limit is $\dot{u}$ the material derivative of u.

Third step. We show the strong convergence of $(u^t - u)/t$. We pass to the limit as $t \to 0$ in (A.4), we show that $\dot{u}$ solves

$$\begin{aligned} \langle \nabla \dot{u}, \nabla v \rangle_{0,\Omega} + \alpha \langle \dot{u}, v \rangle_{0,\Omega} = & - \langle \mathcal{A} \nabla u, \nabla v \rangle_{0,\Omega} - \alpha \langle \mathrm{div}\,(V)\, u, v \rangle_{0,\Omega} + \Big\langle \mathrm{div}\,(V)\, h_2, v \Big\rangle_{0,\Omega} + \langle \nabla h_2 . V, v \rangle_{0,\Omega} \\ & + \langle \mathrm{div}\,(V)\,(h_1 - h_2), v \rangle_{0,\omega} + \langle \nabla (h_1 - h_2).V, v \rangle_{0,\omega}. \end{aligned}$$

This was stated as (A.1) in Theorem A.1. This equation allows us to prove the strong convergence in $H^1(\Omega)$, in fact, taking $v = (u^t - u)/t$ in (A.4), we get

$$\begin{aligned}
\langle A_t\nabla v, \nabla v\rangle_{0,\Omega} + \alpha\langle J_t v, v\rangle_{0,\Omega} &= \Big\langle \frac{I - A_t}{t}\nabla u, \nabla v\Big\rangle_{0,\Omega} + \alpha\Big\langle \frac{1 - J_t}{t}u, v\Big\rangle_{0,\Omega} + \Big\langle J_t\frac{h_2\circ\phi_t - h_2}{t}, v\Big\rangle_{0,\Omega}\\
&\quad + \Big\langle \frac{J_t - 1}{t}h_2, v\Big\rangle_{0,\Omega} + \Big\langle J_t\frac{(h_1\circ\phi_t - h_2\circ\phi_t) - (h_1 - h_2)}{t}, v\Big\rangle_{0,\omega}\\
&\quad + \Big\langle \frac{J_t - 1}{t}(h_1 - h_2), v\Big\rangle_{0,\omega} + \Big\langle \frac{J_t - 1}{t}(h_1 - h_2), v\Big\rangle_{0,\omega}\\
&= \langle (A_t - I)\nabla v, \nabla v\rangle_{0,\Omega} + \alpha\langle (J_t - 1)v, v\rangle_{0,\Omega} + \langle \frac{I - A_t}{t}\nabla u^t, \nabla v\rangle_{0,\Omega}\\
&\quad + \alpha\langle \frac{1 - J_t}{t}u^t, v\rangle_{0,\Omega} + \Big\langle J_t\frac{h_2\circ\phi_t - h_2}{t}, v\Big\rangle_{0,\Omega} + \Big\langle \frac{J_t - 1}{t}h_2, v\Big\rangle_{0,\Omega}\\
&\quad + \Big\langle J_t\frac{(h_1\circ\phi_t - h_2\circ\phi_t) - (h_1 - h_2)}{t}, v\Big\rangle_{0,\omega}\\
&\quad + \Big\langle \frac{J_t - 1}{t}(h_1 - h_2), v\Big\rangle_{0,\omega} + \Big\langle \frac{J_t - 1}{t}(h_1 - h_2), v\Big\rangle_{0,\omega}\\
&= E_{1,t} + E_{2,t},
\end{aligned}$$

we denote by

$$\begin{aligned}
E_{1,t} =& \langle (A_t - I)\nabla v, \nabla v\rangle_{0,\Omega} + \alpha\langle (J_t - 1)v, v\rangle_{0,\Omega},\\
E_{2,t} =& \Big\langle \frac{I - A_t}{t}\nabla u^t, \nabla v\Big\rangle_{0,\Omega} + \alpha\Big\langle \frac{1 - J_t}{t}u^t, v\rangle_{0,\Omega} + \Big\langle J_t\frac{h_2\circ\phi_t - h_2}{t}, v\Big\rangle_{0,\Omega} + \Big\langle \frac{J_t - 1}{t}h_2, v\Big\rangle_{0,\Omega}\\
&+ \Big\langle J_t\frac{(h_1\circ\phi_t - h_2\circ\phi_t) - (h_1 - h_2)}{t}, v\Big\rangle_{0,\omega} + \Big\langle \frac{J_t - 1}{t}(h_1 - h_2), v\Big\rangle_{0,\omega}\\
&+ \Big\langle \frac{J_t - 1}{t}(h_1 - h_2), v\Big\rangle_{0,\omega}.
\end{aligned}$$

Using the weak convergence of $(u^t - u)/t$, we get after straightforward calculations
$E_{1,t} \to 0$ and $E_{2,t} \to -\langle \mathcal{A}\nabla u, \nabla\dot{u}\rangle_{0,\Omega} - \alpha\langle \operatorname{div}(V)\, u, \dot{u}\rangle_{0,\Omega} + \langle \nabla h_2.V, v\rangle_{0,\Omega} + \langle \operatorname{div}(V)\, h_2, \dot{u}\rangle_{0,\Omega} + \langle \nabla(h_1 - h_2).V, v\rangle_{0,\omega} + \langle \operatorname{div}(V)\,(h_1 - h_2), \dot{u}\rangle_{0,\omega}$ when $t \to 0$.
By (A.1), we conclude that $E_{2,t} \to \langle \nabla\dot{u}_d, \nabla\dot{u}_d\rangle_{0,\Omega} + \alpha\langle \dot{u}_d, \dot{u}_d\rangle_{0,\Omega}$.
This shows that $\langle A_t\nabla v, \nabla v\rangle_{0,\Omega} + \alpha\langle J_t v, v\rangle_{0,\Omega}$ converges to $\|\nabla\dot{u}\|^2_{0,\Omega} + \alpha\|\dot{u}\|^2_{0,\Omega}$. Using the proprieties of A_t and J_t we deduce the strong convergence of $v = (u^t - u)/t$ to $\dot{u}$ in $H^1(\Omega)$.

Fourth Step. We obtain the equations satisfied by the shape derivative $u' = \dot{u} - V.\nabla u$. Let $b = (V.\nabla u)\nabla\bar{v} + (V.\nabla\bar{v})\nabla u - (\nabla u.\nabla\bar{v})V$. Using the following classical identity

$$-\nabla u.\mathcal{A}\nabla\bar{v} = \operatorname{div}(b) - (V.\nabla u)\Delta\bar{v} - (V.\nabla\bar{v})\Delta u,$$

and equation (A.1) satisfied by $\dot{u}$ we get

$$\begin{aligned}
\int_\Omega \nabla\dot{u}.\nabla\bar{v} + \alpha\int_\Omega \dot{u}\bar{v} = \int_\Omega \operatorname{div}(b) - \int_\Omega (V.\nabla u)\Delta\bar{v} - \int_\Omega (V.\nabla\bar{v})\Delta u - \alpha\int_\Omega \operatorname{div}(V)\, u\bar{v} + \int_\Omega \operatorname{div}(V)\, h_2\bar{v}\\
+ \int_\Omega \nabla h_2.V\bar{v} + \int_\omega \operatorname{div}(V)\,(h_1 - h_2)\bar{v} + \int_\omega \nabla(h_1 - h_2).V\bar{v}.
\end{aligned}$$

Using the divergence theorem and integration by parts (considering $-\Delta u = -\alpha u + h_2 + (h_1 - h_2)\chi_\omega$), we obtain

$$\begin{aligned}\int_\Omega \nabla \dot{u}.\nabla \bar{v} + \alpha \int_\Omega \dot{u}\bar{v} = &- \int_{\partial\omega} [(V.\nabla \bar{v})\partial_n u] + \int_{\partial\omega} [(\nabla u.\nabla \bar{v})V_n] + \int_\Omega \nabla(V.\nabla u)\nabla \bar{v} \\ &- \alpha \int_\Omega \operatorname{div}(V)\, u\bar{v} + \int_\Omega \operatorname{div}(h_2 V)\, \bar{v} + \int_\omega \operatorname{div}((h_1 - h_2)V)\, \bar{v} \\ &- \alpha \int_\Omega (V.\nabla \bar{v})u + \int_\Omega (V.\nabla \bar{v})h_2 + \int_\omega (V.\nabla \bar{v})(h_1 - h_2).\end{aligned}$$

Which implies that

$$\int_\Omega \nabla(\dot{u} - V\nabla u).\nabla \bar{v}\ dx + \alpha \int_\Omega (\dot{u} - V\nabla u)\bar{v} = -\alpha \int_\Omega (\operatorname{div}(Vu\bar{v}) + \int_\Omega \operatorname{div}(Vh_2\bar{v}) + \int_\omega \operatorname{div}(V(h_1 - h_2)\bar{v}).$$

We obtain the following equation satisfied by the shape derivative $u' = \dot{u} - V.\nabla u$

$$\int_\Omega \nabla u'.\nabla \bar{v} + \alpha \int_\Omega u'\bar{v} = -\int_{\partial\omega} V_n \bar{v}(h_1 - h_2),$$

and using Green's formula we get

$$-\int_\Omega \Delta u'\bar{v} + \alpha \int_\Omega u'\bar{v} - \int_{\partial\omega} \bar{v}\,[\partial_n u'] = -\int_{\partial\omega} V_n \bar{v}(h_1 - h_2).$$

We deduce that u' satisfies the equation $-\Delta u' + \alpha u' = 0$ on $\Omega\backslash\bar{\omega} \cup \omega$ with the condition

$$[\partial_n u'] = (h_1 - h_2)V_n \quad \text{on} \quad \partial\omega.$$

Then, we determine the jump of u'. Since $\dot{u} \in H^1(\Omega)$, we have

$$[u'] = -V_n\ [\partial_n u] = 0 \quad \text{on} \quad \partial\omega.$$

Using the boundary condition $\partial_n u + iu = g + if \quad \text{on} \quad \partial\Omega$ and the fact that $V = 0 \quad \text{on} \quad \partial\Omega$, we obtain

$$\partial_n u' + iu' = 0 \quad \text{on} \quad \partial\Omega.$$

We came to the end of our proof of shape differentiability of u. □

Acknowledgements. We wish to express our gratitude to the editors and referees for their valuable comments and suggestions which helped to improve this paper.

References

[1] L. Afraites, A new coupled complex boundary method (ccbm) for an inverse obstacle problem. *Discrete Contin. Dyn. Syst.-S* **15** (2022) 23.

[2] L. Afraites and A. Atlas, Parameters identification in the mathematical model of immune competition cells. *J. Inverse Ill-Posed Probl.* **23** (2015) 323–337.

[3] L. Afraites, M. Dambrine, K. Eppler and D. Kateb, Detecting perfectly insulated obstacles by shape optimization techniques of order two. *Discrete Contin. Dyn. Syst.-B* **8** (2007) 389.

[4] L. Afraites, M. Dambrine and D. Kateb, Shape methods for the transmission problem with a single measurement. *Numer. Funct. Anal. Optim.* **28** (2007) 519–551.

[5] L. Afraites, C. Masnaoui and M. Nachaoui, Shape optimization method for an inverse geometric source problem and stability at critical shape. *Discrete Contin. Dyn. Syst.-S* **15** (2022) 1.

[6] C.J.S. Alves, R. Mamud, N.F.M. Martins and N.C. Roberty, On inverse problems for characteristic sources in helmholtz equations. *Math. Probl. Eng.* **2017** (2017).

[7] H. Azegami and K. Takeuchi, A smoothing method for shape optimization: traction method using the robin condition. *Int. J. Comput. Methods* **3** (2006) 21–33.
[8] F. Caubet, M. Dambrine, D. Kateb and C.Z. Timimoun, A kohn-vogelius formulation to detect an obstacle immersed in a fluid. *Inverse Probl. Imaging* **7** (2013) 123.
[9] X. Cheng, R. Gong, W. Han and X. Zheng, A novel coupled complex boundary method for solving inverse source problems. *Inverse Probl.* **30** (2014) 055002.
[10] P.J. Daniell, Lectures on cauchy's problem in linear partial differential equations. *Math. Gaz.* **12** (1924) 173–174.
[11] R. Dautray and J.-L. Lions, Mathematical Analysis and Numerical Methods for Science and Technology: Volume 3 Spectral Theory and Applications, Vol. 3. Springer Science & Business Media (1999).
[12] M.C. Delfour and J.-P. Zolésio, Shapes and Geometries: Metrics, Analysis, Differential Calculus, and Optimization. SIAM (2011).
[13] A. El Badia and T.H. Duong, Some remarks on the problem of source identification from boundary measurements. *Inverse Probl.* **14** (1998) 883.
[14] A. El Badia and T. Nara, An inverse source problem for helmholtz's equation from the cauchy data with a single wave number. *Inverse Probl.* **27** (2011) 105001.
[15] K. Eppler and H. Harbrecht, A regularized newton method in electrical impedance tomography using shape hessian information. *Control Cybern.* **34** (2005) 203.
[16] M. Giacomini, O. Pantz and K. Trabelsi, Certified descent algorithm for shape optimization driven by fully-computable a posteriori error estimators. *ESAIM: Control Optim. Calc. Var.* **23** (2017) 977–1001.
[17] R. Gong, X. Cheng and W. Han, A coupled complex boundary method for an inverse conductivity problem with one measurement. *Appl. Anal.* **96** (2017) 869–885.
[18] J. Haslinger and R.A.E. Mäkinen, Introduction to Shape Optimization: Theory, Approximation, and Computation. SIAM (2003).
[19] F. Hecht, Finite Element Library Freefem++.
[20] M. Hrizi and M. Hassine, One-iteration reconstruction algorithm for geometric inverse source problem. *J. Elliptic Parabol. Equ.* **4** (2018) 177–205.
[21] R. Kress and W. Rundell, A nonlinear integral equation and an iterative algorithm for an inverse source problem. *J. Integral Equ. Appl.* **27** (2015) 179–198.
[22] V. Michel and A.S. Fokas, A unified approach to various techniques for the non-uniqueness of the inverse gravimetric problem and wavelet-based methods. *Inverse Probl.* **24** (2008) 045019.
[23] F. Murat and J. Simon, Sur le contrôle par un domaine géométrique. *Rapport du LA* **189** (1976) 76015.
[24] A. Oulmelk, L. Afraites, A. Hadri and M. Nachaoui, An optimal control approach for determining the source term in fractional diffusion equation by different cost functionals. *Appl. Numer. Math.* **181** (2022) 647–664.
[25] M. Pierre and A. Henrot, Shape Variation and Optimization: A Geometrical Analysis (2018).
[26] J.F.T. Rabago, On the new coupled complex boundary method in shape optimization framework for solving stationary free boundary problems. Preprint arXiv:2205.12620 (2022).
[27] N.C. Roberty and C.J.S. Alves, On the identification of star-shape sources from boundary measurements using a reciprocity functional. *Inverse Probl. Sci. Eng.* **17** (2009) 187–202.
[28] J.-P. Zolésio and M.C. Delfour, Shapes and Geometries: Analysis, Differential Calculus, and Optimization. SIAM (2001).